HST Far-Ultraviolet Imaging of Jupiter During the Impacts of Comet Shoemaker-Levy 9

John T. Clarke, Renée Prangé, Gilda E. Ballester, John Trauger, Robin Evans, Daniel Rego, Karl Stapelfeldt, Wing Ip, Jean-Claude Gérard, Heidi Hammel, Manish Ballav, Lotfi Ben Jaffel, Jean-Loup Bertaux, David Crisp, Claude Emerich, Walter Harris, Mihaly Horanyi, Steven Miller, Alex Storrs, Harold Weaver

Hubble Space Telescope far-ultraviolet images of Jupiter during the Shoemaker-Levy 9 impacts show the impact regions darkening over the 2 to 3 hours after the impact, becoming darker and more extended than at longer wavelengths, which indicates that ultraviolet-absorbing gases or aerosols are more extended, more absorbing, and at higher altitudes than the absorbers of visible light. Transient auroral emissions were observed near the magnetic conjugate point of the K impact site just after that impact. The global auroral activity was fainter than average during the impacts, and a variable auroral emission feature was observed inside the southern auroral oval preceding the impacts of fragments Q1 and Q2.

The ~20 separate bodies from the disrupted comet Shoemaker-Levy 9 impacted Jupiter's predawn southern hemisphere (*1*) between 16 and 22 July 1994. Entering at a relative speed of 60 km s^{-1} and a zenith angle of 45°, the fragments deposited large amounts of energy into Jupiter's atmosphere. Many of the impact plumes rose 2000 to 3000 km above the visible cloud tops (*2*). The cooling material then spread laterally and fell, with the particles and molecules diffusing through the atmosphere with vertical diffusion rates determined by the state of the atmosphere. The high initial temperature of the plumes (*3*) probably dissociated most of the molecules, with consequent recombination and photochemistry occurring as the plumes rose and cooled.

Many of the cometary and atmospheric constituents that were anticipated in the impact plumes are strong absorbers at far-ultraviolet (FUV) wavelengths. Preimpact models of the passage of the fragment bodies through Jupiter's magnetosphere (*4*) also suggested that several mechanisms could produce observable effects in Jupiter's aurora or ionosphere, including the effects of the extended dust cloud on Jupiter's magnetosphere and electrodynamic effects associated with the rapid cross-field motion of the fragments. We therefore acquired FUV images of Jupiter to (i) study the response of Jupiter's upper atmosphere to the impacts, (ii) measure upper atmospheric winds through observed motions of impact-related absorbers, and (iii) search for auroral emissions associated with the comet material passing through Jupiter's magnetosphere or from the aftereffects of the impacts. Before these observations, there had been no direct measurements of the winds in Jupiter's upper atmosphere (at pressures $p < 1$ to 10 mbar) (*5*), and Jupiter's FUV aurorae have only been imaged recently by the Hubble Space Telescope (HST) (6). A new capability for FUV imaging of Jupiter's aurora with the HST Wide Field Planetary Camera 2 (WFPC2) and the post-COSTAR (Corrective Optics Space Telescope Axial Replacement) Faint Object Camera (FOC) is presented in this paper. This is necessarily a progress report, after just 3 months of analysis, and more detailed reports on these images will be presented at a later time.

J. T. Clarke, G. E. Ballester, M. Ballav, and W. Harris are at the Space Physics Research Laboratory, University of Michigan, Ann Arbor, MI 48109, USA. R. Prangé is at the Institut d'Astrophysique Spatiale, CNRS–Université Paris XI, 91405 Orsay Cedex, and the Institut d'Astrophysique de Paris, CNRS, 75014 Paris, France. J. Trauger, R. Evans, K. Stapelfeldt, and D. Crisp are at the Jet Propulsion Laboratory, Pasadena, CA 91109, USA. D. Rego is at the Space Physics Research Laboratory, University of Michigan, Ann Arbor, MI 48109, USA, and the Institut d'Astrophysique Spatiale, CNRS–Université Paris XI, 91405 Orsay Cedex, France. W. Ip is at the Max-Planck-Institut für Aeronomie, D-37191 Katlenburg-Lindau, Germany. J.-C. Gérard is at the Institut d'Astrophysique, Université de Liège, 4000 Liège, Belgium. H. Hammel is at Massachusetts Institute of Technology, Cambridge, MA 02139, USA. L. B. Jaffel is at the Institut d'Astrophysique de Paris, CNRS, 75014 Paris, France. J.-L. Bertaux is with the Service d'Aeronomie du CNRS, Verrieres le Buisson, 91371 France. C. Emerich is at the Institut d'Astrophysique Spatiale, CNRS–Université Paris XI, 91405 Orsay Cedex, France. M. Horanyi is with LASP, University of Colorado, Boulder, CO 80309, USA. S. Miller is with the Department of Physics and Astronomy, University College, London, UK. A. Storrs and H. Weaver are at the Space Telescope Science Institute, Baltimore, MD 21218, USA.

Observations and Data Reduction

The FUV images of Jupiter were obtained with both the WFPC2 and the FOC between 13 July and 9 August 1994. The FUV images were scheduled 3 days before the impacts, within 2 to 4 hours after two of the first five impacts, one and three jovian rotations after the first images, then at roughly daily intervals spaced throughout the remaining week, and finally 1 and 2 weeks after the impacts ended. The timing intervals were planned to determine the time scales for auroral and impact site changes. Because of the longer integration times required for the FUV images and the expectation of short-lived plume phenomena, all images during impacts used visible or near-UV filters by agreement with the HST visible imaging team. The limited time for FUV imaging dictated that we concentrate on the side of Jupiter near a central meridian longitude (CML) = 180° (System III). This side afforded the best view of the northern auroral zone, sometimes showing the extensions of magnetic field lines from the impact sites to the northern hemisphere (the magnetic conjugate points) even when the impacts occurred beyond the limb, and offered a time series of the development of the C, A, and E impact sites (*7*). We later obtained images of opposite sides of Jupiter spaced half of a jovian rotation apart to record nearly the full range of impact sites on 21 July (after the R impact) and on 9 August (after all impacts). We also obtained images shortly after the K impact (expected to be one of the larger fragments) and a series of four images just before the impact of fragment P2. The latter two image series were intended to search for fragment-induced auroral emissions.

Each WFPC2 imaging set consisted of a pair of exposures with the Wide Field Camera (WFC) with the filters F160BW (1150 to 2100 Å) and F160BW + F130LP (1300 to 2100 Å). This approach facilitated cosmic ray identification and removal and the isolation of the shortest wavelength emissions (including H Lyman α) as a difference of images. Comprehensive discussions of the properties of the WFPC2 and image reduction are presented elsewhere (*8*). Cosmic ray events typically deposit 10 times more charge per pixel than Jupiter and are readily identified by the deviation from the median of neighboring pixel values. The final test of the reality of any small-scale feature in WFPC2 images is the appearance of the feature in each of a pair of images, because the cosmic ray coincidence rate is low. No spatial filtering has been performed on WFPC2 images. Locations on Jupiter in the FUV images have been determined by an edge-finding algorithm (9). For the WFPC2 images, we estimate positional uncertainties on Jupiter of less than 100 km when visible and FUV frames are taken on the same guide stars, and ~300 km for isolated FUV exposures (1 WFC pixel = 0.1 arc sec). Jupiter's rotation also imposes a longitudinal blurring in proportion to the exposure length. The FOC images (*10*) were taken with the combination of filters F152M and F175W to isolate the long wavelength end of the auroral H_2 Lyman band emissions, which is least sensitive to atmospheric CH_4 absorption. The residual transmission of the filter combination ("red leak") was used to map the jovian disk in the Rayleigh-scattered solar flux. The field of view of FOC (14 arc sec by 14 arc sec) is smaller than that of WFPC2 and only permits mapping of the mid- to high-latitude region of one hemisphere at a time. By contrast, its high spatial sampling rate (zoomed pixel size = 0.014 arc sec by 0.028 arc sec) allows the detection of localized emission features such as those related to auroral field-aligned currents.

Every FUV image taken after 16 July showed large dark regions at the locations of fragment impacts. An overview of the FUV absorption regions is shown in Fig. 1, with two images obtained one-half of a jovian rotation apart on 21 July (after the R impact), and a projection of the southern latitudes from these images to a cylindrical grid of longitude and latitude (*11*). The effective wavelength of the nonauroral part of the FUV images can be estimated by folding an IUE spectrum of Jupiter's equator through the estimated instrument response. For WFPC2 with the F160BW filter, we derive a bandpass with half-power points at 1760 and 2070 Å and a central wavelength of 1900 Å. The blue and near-UV (*12*) images (Fig. 1B) have effective wavelengths of 2760 Å for the F255W filter and 3350 Å for F336W. There is a negligible contribution in the F160BW images from light above 2200 Å. The FOC half-maximum bandpass with filters F152M and F175W is 1460 to 1670 Å. When folded with Jupiter's reflection spectrum, it peaks near 2000 Å with significant sensitivity up to visible wavelengths. The effective bandpasses for the impact sites are uncertain by the relative difference in spectrum: IUE spectra suggest that the impact site effective wavelengths may be up to 50 to 100 Å greater than the estimates based on equatorial spectra.

Impact Site Images

The distribution and extent of the FUV darkening at the impact sites (Fig. 1A) can be compared with their appearance (*2*) at blue and near-UV wavelengths (Fig. 1B). The impact regions appear considerably darker and more extended in the FUV, partly because of the classical or "normal" darkening at both poles on Jupiter. Models of Jupiter's near-UV spectrum show that the observed albedo is fit well by a combination of Rayleigh-Raman scattering and particulate absorption down to 2200 to 2300 Å, and at shorter wavelengths, molecular photoabsorption contributes strongly to the observed decreasing albedo (*13*). Jupiter's "polar hoods" appear dark (*14*) from the shortest wavelengths to around 3000 Å; this darkening is attributed to complex hydrocarbons and other molecular absorbers resulting from enhanced auroral photochemistry (*15*). As examples, 1700 Å photons reach unit optical depth at atmospheric pressures of only ~0.1 to 1 mbar or 200 to 300 km above the ammonia cloud deck because of high-altitude C_2H_2 absorption, whereas 2100 Å photons reach unit optical depth at ~100 mbar or a height of 50 km. The FUV images therefore sample a large range of altitudes in Jupiter's stratosphere. Any fragment constituents or lower atmospheric gas injected into Jupiter's atmosphere above the 100-mbar level could produce FUV darkening, and most simple molecules absorb more strongly in the FUV than at visible wavelengths. The FUV images therefore place constraints on the vertical and horizontal distribution, composition, and lifetime of the high-altitude absorbers.

We estimated the time scale of the FUV darkening in these images. In the first image of the fragment C impact site 2.2 hours after the impact (second frame from bottom in Fig. 2), the C feature appeared less dark and nearly separated into two components in latitude. One jovian rotation later, this feature was as dark as the A and E features, and the E feature (4.0 hours after impact) was also fully dark at this time. Images of the K impact site ~50 min after impact (Fig. 3) show that this region also was not as dark as it would become later. The time scale for the FUV darkening of the impact regions appears to be on the order of 2 to 3 hours. This is consistent with the decreasing albedo measured in a series of IUE spectra of the E and G features 1 to 4 hours after the impact (*16*) and also FOS spectra of the G feature (*17*). The darkening time scale may be explained in part by increased absorption by simple molecules formed by recombination as the plume material expands and cools, and in part by atmospheric absorbers convectively lifted into the stratosphere from the heat released in the impact. In view of the large extent of the

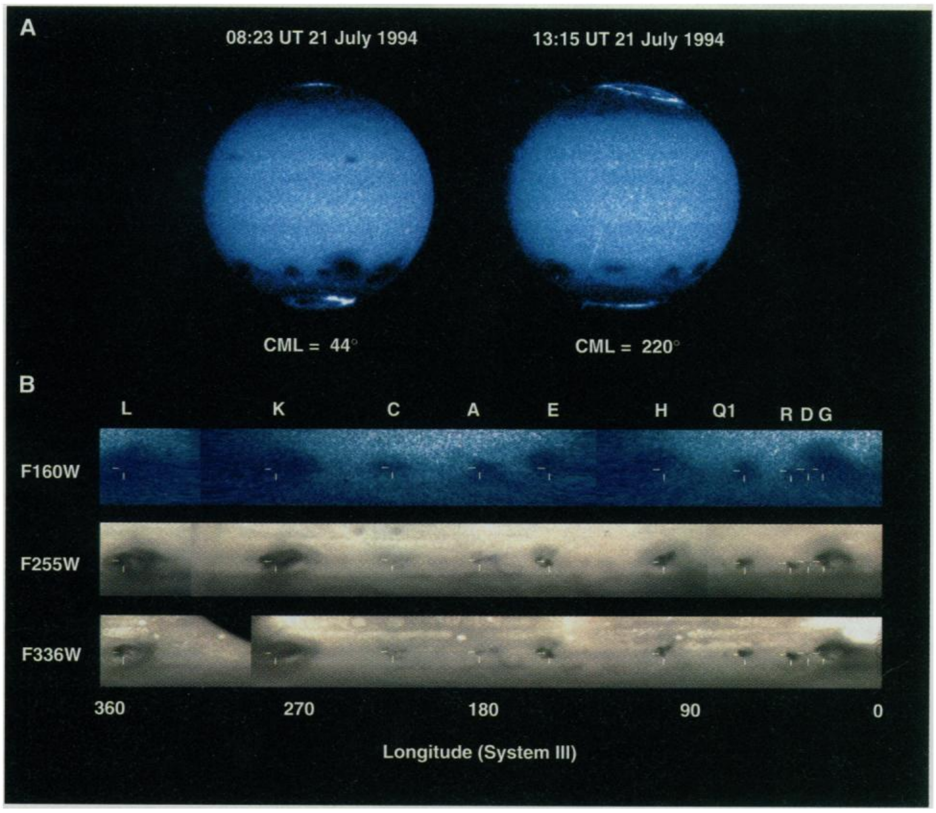

Fig. 1. (**A**) Two WFPC2 FUV images taken 5 hours apart on 21 July 1994 showing nearly the whole Jupiter disk; northern mid-latitude dark features are Io and its shadow. (**B**) Regions centered at −45° latitude in a cylindrical projection. Images from filters F255W and F336W were taken within 12 hours of the F160W images; crosshairs mark the impact sites determined from HST visible imaging (*2*).

absorbing regions, and their motions discussed later, we initially give more weight to the former process. This darkening time scale in the FUV contrasts that of visible images, in which the impact sites appear dark as soon as they rotate into view, suggesting that additional FUV absorbing material is formed or raised into the upper atmosphere in addition to the visible material from the plume.

Drift motions of the C, A, and E impact features are displayed in Fig. 2. Although the feature centers were nearly fixed in System III longitude, as had previously been observed for visible cloud features at this latitude, by 29 July all three impact features were extended in longitude beyond the image blurring expected as a result of Jupiter's rotation (*18*). An additional complex north of the A and E features also appears in the 29 July and 9 August images, and the B to G features are extended in longitude on 9 August with an additional complex north of the Q2-R complex (Fig. 4). Examination of these images and other WFPC2 F255W images shows that the absorbing features north of the A-E complex evolved from the E feature, which extended toward the north for 3 to 6 days after the impact, then stopped moving north and extended east to west. An additional feature just northeast of the E impact site can also be seen in the 29 July image; this feature also appears in the blue and near-UV images, but the more northern feature does not. Each feature appears less dark in the 29 July image, which may largely be the result of the longitudinal spread of the absorbing material.

For quantitative measurements of the FUV absorption and changes with time, we plotted a series of north-south intensity traces (Figs. 5 and 6), where absorption is indicated by the difference of the intensities across the impact site and the neighboring atmosphere. Figure 5 compares FUV and blue (F336W) bandpasses on the C and E sites 4 hours after the E impact and on the G and K sites later in the week. The absorption in the FUV was stronger and more extended than that at visible wavelengths, in addition to the more pronounced FUV limb darkening near the south pole. Some FUV clouds also appeared offset from the visible clouds (Figs. 1 and 5). In particular, the E, D-G, and K features appeared offset to the north, whereas the A, Q1, and L features were centered or slightly offset to the south. The largest impacts, in particular, the G, L, and K impacts, spread FUV absorbing material initially over the largest areas. In comparisons of the FUV and longer wavelength images (Fig. 5), the FUV absorbing material extends well beyond the visible material.

We searched in the FUV images for a stronger central absorption core similar to the structure seen in visible images and found no indication of this in the C, A, or E features at 0.1–arc sec resolution. The FUV absorption features appear to be diffuse regions, with central absorption optical depths near $\tau = 1$ for C, A, and E to near zero intensity for G and K. The relative absorptions in Figs. 5 and 6 indicate line-of-sight columns into the atmosphere (weighted over the bandpass) determined by a combination of H_2 Rayleigh scattering, additional scattering and absorption from impact-induced particles, and molecular photoabsorption in the impact region. In the impact regions, the $\tau = 1$ level may be at relatively higher altitudes than outside these regions, because of absorbing material diffusing through the atmosphere after a plume event. The lack of central absorption structure, the large and diffuse appearance, and our knowledge of Jupiter's albedo at these wavelengths all suggest that the impact-site FUV bandpass was dominated by absorption at altitudes higher than that of most of the particles; particulate scattering progressively dominates as one moves to longer wavelengths (*12*).

Some preliminary estimates of Jupiter's upper atmospheric winds can be derived from the evolution of the C, A, and E features with time (Fig. 6). Despite the noise in these intensity traces, some trends appeared in more than one impact site. There was initially a southern extension of the absorption in each feature, most pronounced in the C feature (which was observed closest to the time of impact) and extending in the case of the A feature a full 2 arc sec south of the impact site. This southern absorption remained 1 day after

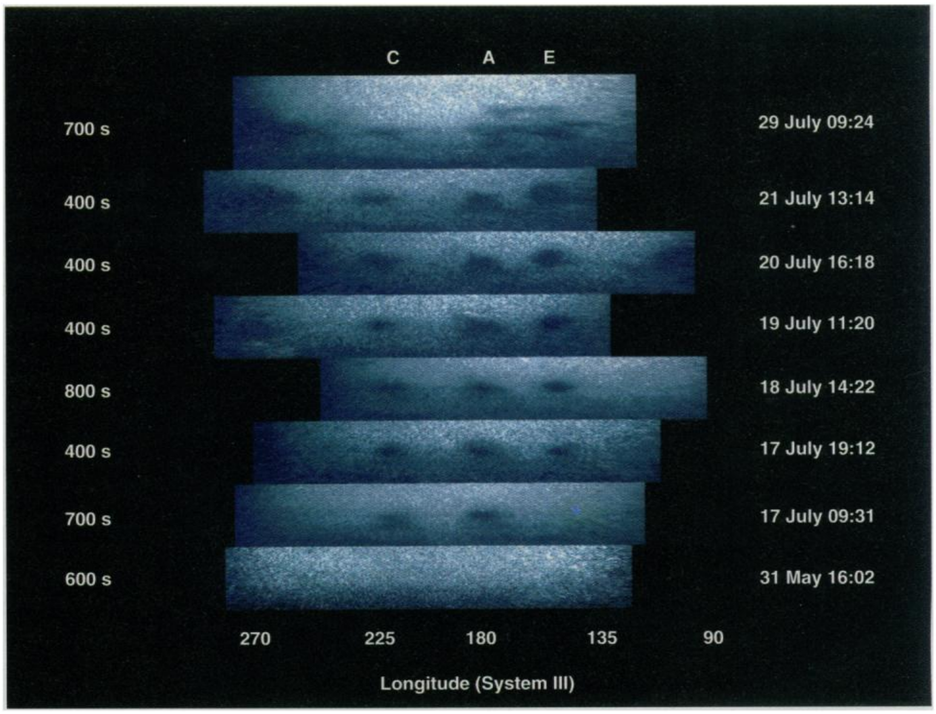

Fig. 2. Series of WFPC2 FUV image segments from southern latitudes during the period of impacts in a cylindrical projection plotted versus System III longitude, showing relative drift motions and evolution of the C, A, and E impact sites. All images were taken with filter F160BW; the times given to the right are for the midpoint of each exposure, the lengths of which are given to the left.

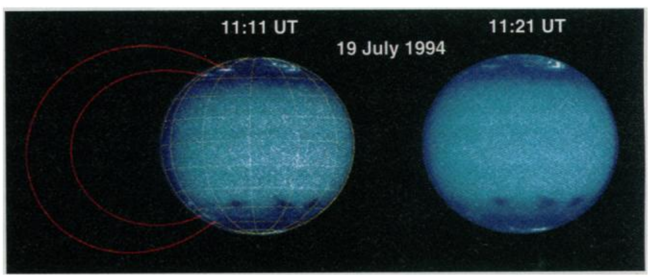

Fig. 3. WFPC2 FUV images taken 47 and 57 min after the K impact (assumed at 10:24 UT), showing auroral emissions at lower latitudes than normally observed and apparently associated with the K impact event. The left image has magnetic field lines overplotted from the O_6 model (*22*) showing the extension of the northern emission centers to near the K impact region in the southern hemisphere. The left image was for 400 s with filters F160BW and F130LP, the right image for 400 s with F160BW.

the A and C impacts and had dissipated in all cases within 2 days after each impact. The motion needed to transport material in the C feature south by ~6000 km in <2.2 hours is >1 km s^{-1}. This appears to be partly the result of the initial plume sending an extended component south, although it is not yet clear why the extended absorption dissipated within 2 days while the central absorption remained for more than 10 days. The vertical diffusion time scale down through the expected line-of-sight column at 1900 Å is large compared with 2 days (*19*), suggesting some active dissipation process for this material. It seems plausible that the southern-extending material may have been dissipated by upper atmospheric winds. Over the first 3 days following the impact, the E feature extended to the north and would have continued north for another 3 days to reach the observed −32° latitude, after which most of its spreading became east to west. The initial northern motion from the northern half-power point of the absorption feature was on the order of 50 m s^{-1}.

Impact-Related Auroral Emissions

An additional goal of our program was to search for auroral changes accompanying the dust cloud in Jupiter's magnetosphere, the passage of the fragments through the magnetic field, and effects from the impacts themselves. Although IUE has been studying Jupiter's aurora spectroscopically since 1979 (*20*), the field of FUV imaging of Jupiter's aurora is young, having begun with the HST FOC images of the aurora in 1992 (*6*). The first FUV images of Jupiter's aurora were obtained with WFPC2 in May 1994 and with the post-COSTAR FOC in June 1994, so that we now have a sufficient number of high-quality FUV images of Jupiter to establish at least a limited baseline for the "normal" spatial distribution and brightness of the aurora (*6*). The distribution of polar auroral emissions on Jupiter can be seen in Figs. 1 and 4, with each image showing an oval structure associated with one of the magnetic poles when that pole is oriented toward Earth. The aurora has consistently been observed to exhibit an oval form in both FOC and WFPC2 images, although often with considerable structure and brightness variations along this oval. The recent images have also shown that there is commonly diffuse emission inside the ovals and sometimes emission structures extending down to the magnetic flux tubes 6 jovian radii from the planet (at $6R_J$) and down to the Io flux tube.

Overall, Jupiter's FUV aurora appears to have been fainter than average 1 week before and during the week of impacts in both the WFPC2 and FOC images, although within the range of variation observed over 15 years of IUE spectra (*21*). Although some decrease in overall auroral activity was predicted because of the damping effect of the extended dust cloud on magnetospheric plasma, the significance of the fainter-than-average aurora is presently unclear because it was within the previously observed range of variation. The auroral morphology during the impacts was similar to that before the impacts (Fig. 4).

A less ambiguous case of atypical auroral emissions is displayed in Fig. 3, showing two images obtained 47 and 57 min after the K impact. Discrete mid-latitude auroral emissions were detected near the approaching limb and well separated from the "normal" auroral oval, connected to magnetic field lines extending out to $2R_J$ within the region of intense synchrotron radio emission from Jupiter's radiation belts. The two northern emission arcs appeared from (latitude, longitude) +51°, 257° to +52°, 277° and +56°, 238° to +56°, 258°. While the northern emissions are evident in both images in Fig. 3, we also identify fainter but significant emissions just south of the K impact site. Emission is seen between −54°, 275° and −52°, 280°, which appears to be consistent with the conjugate point of the brighter of the northern emissions within the uncertainty in the field model (*22*), although the northern hemisphere emission appears at significantly greater longitudes (potentially as a result of plasma drift while traveling to the northern hemisphere). At the southern conjugate point of the lower latitude northern feature, a cosmic ray obscured the region in the first image, and no emission was detected in the second image. For a K impact at −43.8°, 279°, no emission was detected from the northern conjugate point at +38°, 269°. Although the southern emissions appeared 2 to 3 times fainter than the northern emissions, they came from an area with unusual FUV absorption from the K impact, so that the true

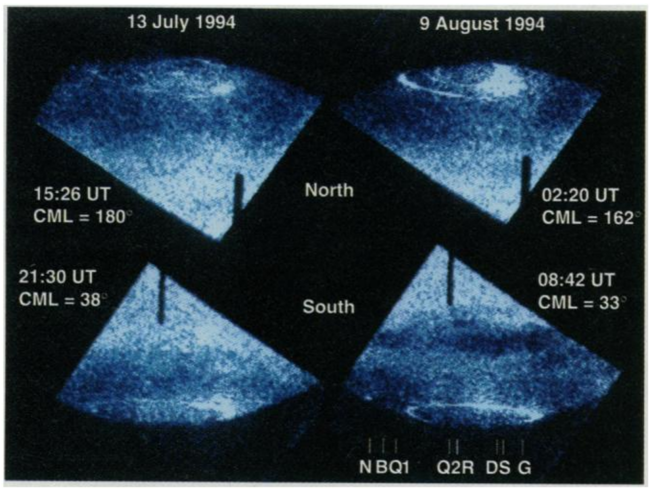

Fig. 4. FOC FUV images obtained on 13 July (during dust infall) and 9 August (~2 weeks after last impact and the last FUV image obtained) showing similar auroral morphology but fainter emissions during dust infall. Longitudinally extended impact sites N to G can be seen in the southern image from 9 August. The dark, vertical linear feature on the disk is the occulting finger of the FOC.

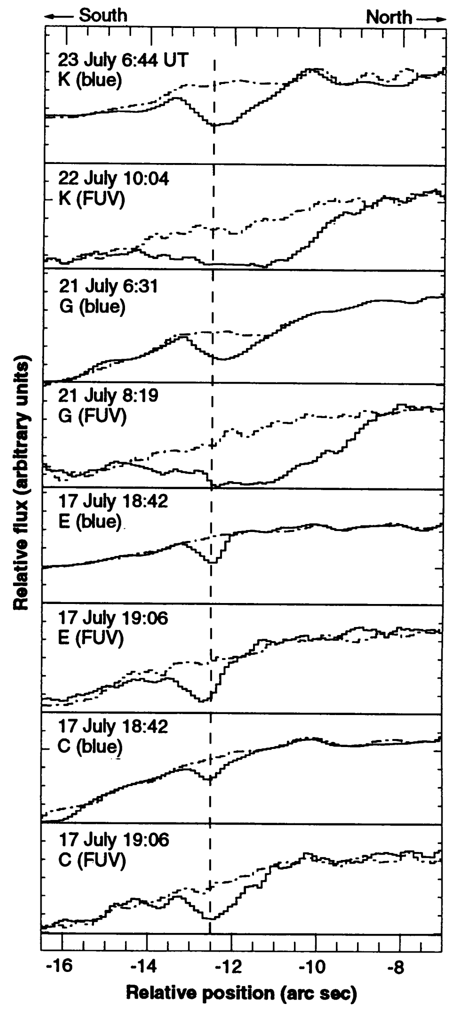

Fig. 5. Line plots of intensity in strips 1 arc sec wide passing north-south across the C, E, G, and K impact sites (solid lines) and across nearby regions free of impact darkening (dotted lines) in WFPC2 FUV images, compared with the visible F336W image taken closest in time to the FUV image. Note that 0.1 arc sec corresponds to ~370 km at Jupiter's distance during the week of impacts.

ratio of auroral excitation north-south may have been closer to unity than observed. More detailed knowledge of the altitudes of the emissions and absorbers will be needed to pursue this question. Finally, the emissions decreased with time between the two images. The maximum surface brightness (*23*) of the brighter of the two northern emission features was 250 kilorayleighs (kR), decreasing to 180 kR in the second image (taken with a higher sensitivity filter combination), with a half-maximum width of 2000 km by 25,000 km.

The excitation of these emissions appears to be associated with the K impact event, from a combination of timing and the approximate magnetic conjugacy with the K impact site. There has also been reported a burst of x-ray emission from the northern hemisphere detected by ROSAT (*24*). This burst appeared within minutes of the K impact event, lasted a few minutes, and required a power input $\sim 10^{13}$ to 10^{16} W of high-energy charged particles for the production of x-rays either by electron bremsstrahlung or O and S ion K-shell excitation. The IUE spectra of the K impact site in the south also revealed enhanced H_2 band emissions at the time of the impact (*16*). There may have been a simultaneous burst of FUV emission at the time and location of the x-ray burst; however, there were no FUV observations of the northern site during the impact. In addition, Jupiter's synchrotron radiation was observed to increase over the week of impacts, while the position of the emission peaks east and west of the planet moved closer to Jupiter (*25*), suggesting some disturbance of the trapped charged-particle population in Jupiter's radiation belts.

We have considered the following possible processes for the production of the FUV emissions after the K impact. (i) The disturbance in the K impact region very likely produced local heating in the ionosphere, which could have produced a stream of plasma directed out along the magnetic field by analogy to similar processes at the Earth (*26*). (ii) The initial burst of emission may have been caused by scattered particles from the radiation belt [suggested by Waite *et al.* (*24*)], and the FUV emissions observed 50 min later could have been a combination of residual emission from the burst (that is, ongoing electrojet currents initiated by the burst) plus incident streaming plasma from the impact site arriving after the initial burst. For example, the production of an electromagnetic disturbance in the K impact channel or surrounding ionosphere might have created Whistler mode or Alfvén waves that propagated along the magnetic field and directly scattered or initiated the growth of plasma waves within the radiation belts. (iii) Dessler and Hill (*27*) have proposed that an ionospheric dynamo induced by strong thermospheric winds moving out from the impact site could induce field-aligned currents that would close in the northern ionosphere, producing the observed emissions. This appears consistent with the observed geometry and location of the emissions, although it is not clear why bright emissions would only be observed poleward of the impact site. We consider each of these scenarios to be plausible; however, at this time it is not possible to state conclusively how the FUV emissions were produced.

Finally, we present in Fig. 7 the southern aurora in a series of four FUV images obtained shortly before the P2 impact, showing a variable auroral emission near the far side of the auroral oval. This emission appears to be "blinking" on and off in this series of images, taken over roughly 10-min intervals, which is not an artifact of different filter responses or other instrumental effects. The feature brightness (*23*) above the neighboring part of the auroral oval in the four images is ~200, <20, ~240, and <20 kR, compared with a peak auroral brightness near the receding limb of ~300 kR in the first two images with ~500 kR in the second pair. In the "off" images, the upper limit is set by the observed brightness of the auroral oval at the location of the feature. Such variability has not been ob-

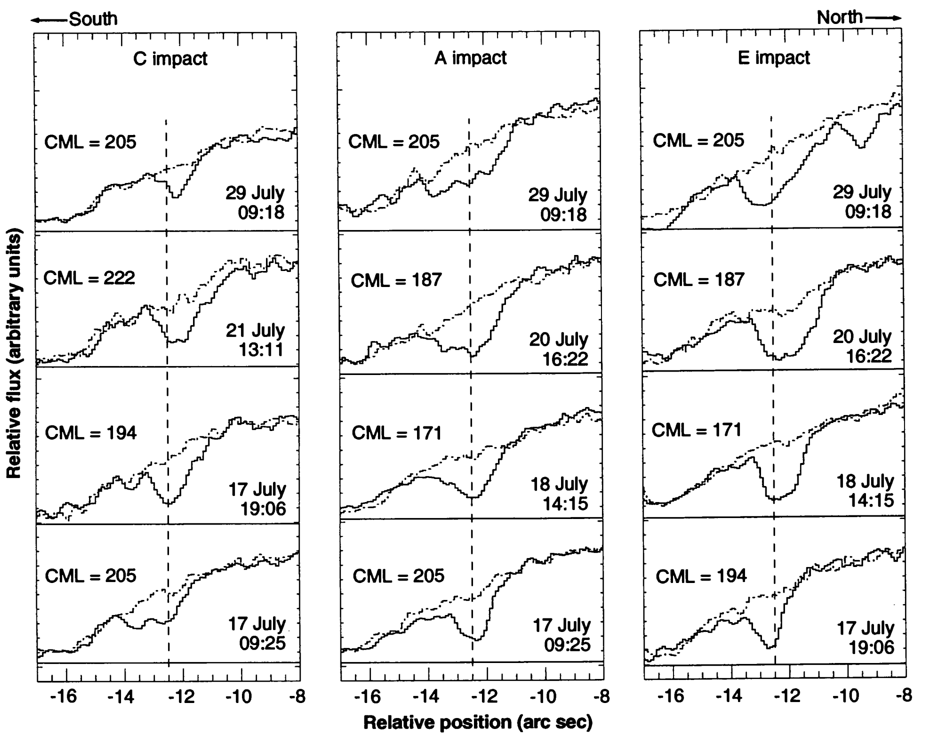

Fig. 6. Line plots of intensity in strips 1 arc sec wide passing north-south across the C, A, and E impact sites (solid lines) with respect to nearby regions free of impact darkening (dotted lines), showing the evolution of FUV absorption in WFPC2 images with filter F160BW.

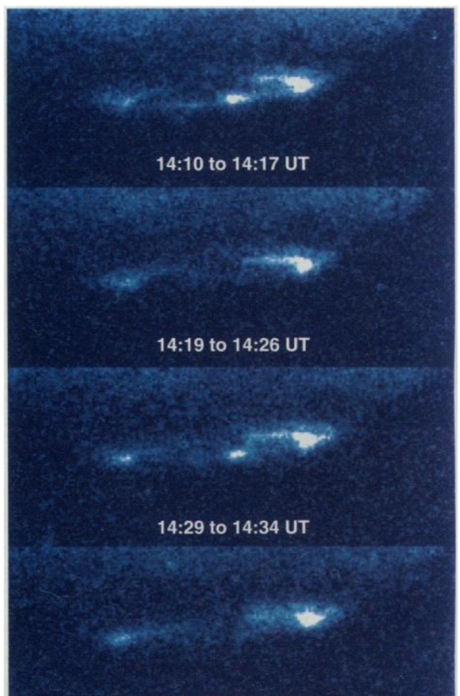

Fig. 7. Southern section of four WFPC2 FUV images (logarithmic stretch) from 20 July as fragment P2 approached Jupiter. Note the variable emission from the far section of the southern auroral oval. The first two images were 400-s exposures with filters F160W and F130LP; the second two were 300-s exposures with filter F160W. Central meridian longitudes at midexposure were 107°, 112°, 118°, and 125°, top to bottom.

served in any other FOC or WFPC2 images to date, raising the possibility that this feature is related to the approaching comet fragments. An analysis of this emission feature and magnetic field tracing are presented by Prangé *et al.* (*28*).

REFERENCES AND NOTES

1. C. S. Shoemaker, E. M. Shoemaker, D. H. Levy, *Int. Astron. Union Circ. 5725* (1993); J. V. Scotti and H. J. Melosh, *Nature* **365**, 733 (1993); D. K. Yeomans and P. Chodas, *Minor Planet Circ. 22197* (1993).
2. H. B. Hammel *et al.*, Science **267**, 1288 (1995).
3. M. B. Boslaugh, D. A. Crawford, A. C. Robinson, T. G. Trucano, *Geophys. Res. Lett.* **21**, 1555 (1994).
4. F. Herbert, *ibid.*, p. 1047; W. H. Ip and R. Prangé, *ibid.*, p. 1051; P. Kellog, *ibid.*, p. 1055; O. Bolin and N. Brenning, *ibid.*, p. 1063; W. Farrell *et al.*, *ibid.*, p. 1067.
5. J. Sommeria, L. Ben Jaffel, R. Prangé, in preparation.
6. V. Dols *et al.*, *Geophys. Res. Lett.* **19**, 1803 (1992); J. Caldwell *et al.*, *Science* **257**, 1512 (1992); J. C. Gérard, V. Dols, F. Paresce, R. Prangé, *J. Geophys. Res.* **98**, 18793 (1993); J. T. Clarke *et al.*, in preparation.
7. Fragment designations are given by H. A. Weaver *et al.*, *Science* **267**, 1282 (1995).
8. J. T. Trauger *et al.*, *Astrophys. J.* **435**, L3 (1994); J. Holtzman *et al.*, *Publ. Astron. Soc. Pac.*, in press. Images were reduced by (i) subtraction of a flat bias level and scaled dark frames, (ii) division by a flat field image including the detector pixel to pixel response, telescope illumination pattern, and Wood's filter vignetting, and (iii) cosmic ray removal. Finally, the images were corrected for geometric distortion and image shift introduced by the MgF_2 field flattener on the charge-coupled device (CCD) detectors.
9. The edge-finding algorithm consists of (i) finding points of inflection in radial intensity scans over a range of angles on the sunlit limb, (ii) shifting a projected oblate spheroid (an ellipse) of the proper shape, angle, and size of Jupiter in *x* and *y* to obtain the statistical best fit to the edge points, and (iii) correcting the east-west location by a measured systematic shift of the observed inflection points from the true limb from a model of the instrument point spread function and limb darkening of Jupiter.
10. As part of the standard data processing, the FOC images were flat fielded and corrected for the geometric distortion resulting from the optical elements and the detector. Locations on Jupiter are determined in the same way as for WFPC2, except that the FOC response provides the polar limb, which can be fit with a model oblate spheroid. A preliminary processing was applied to improve the visibility of features against the noise with a two-dimensional spatial filtering code based on a comparison of counts on Jupiter with the statistics in a background region.
11. A small amount of limb brightening has been added in the lower plots to assist viewing of the absorption regions, rather than correcting for the actual limb darkening.
12. R. A. West *et al.*, *Science* **267**, 1296 (1995).
13. R. Wagener *et al.*, *Icarus* **63**, 222 (1985).
14. W. R. Pryor and C. W. Hord, *ibid.* **91**, 161 (1991).
15. R. Wagener and J. Caldwell, *ibid.* **74**, 141 (1988).
16. W. M. Harris *et al.*, in preparation; R. Prangé *et al.*, *Int. Astron. Union Circ. 6040* (1994); W. Harris *et al.*, *ibid.*; G. Ballester *et al.*, in preparation.
17. K. Noll *et al.*, *Science* **267**, 1307 (1995).
18. At Jupiter's rotation rate of 36°/hour, the rotational smearing in the 400- to 800-s exposures was 4° to 8° in longitude.
19. T. E. Cravens, *Geophys. Res. Lett.* **21**, 1075 (1994).
20. J. T. Clarke, H. W. Moos, S. K. Atreya, A. L. Lane, *Astrophys. J.* **241**, L179 (1980).
21. W. M. Harris *et al.*, in preparation; T. A. Livengood, D. F. Strobel, H. W. Moos, *J. Geophys. Res.* **95**, 10375 (1990).
22. J. E. P. Connerney, in *Planetary Radio Emission*, H. Rucker, M. L. Kaiser, S. J. Bauer, Eds. (Austrian Academy of Science Press, Vienna, 1992), vol. 3, p. 13; personal communication. Magnetic field estimates are for the O_6 model plus current sheet.
23. Brightnesses are estimated for the emissions included in each bandpass using a preliminary estimate for the mean sensitivity at the time of comet impacts (10 days after the most recent WFPC2 decontamination) of 0.0045 electrons s^{-1} per WFC pixel for a 10-kR emission.
24. J. H. Waite *et al.*, *J. Geophys. Res.* **99**, 14799 (1994); J. H. Waite *et al.*, in preparation.
25. I. De Pater *et al.*, in preparation.
26. T. I. Gombosi and A. F. Nagy, *J. Geophys. Res.* **94**, 359 (1989).
27. A. J. Dessler and T. W. Hill, *Bull. Am. Astron. Soc.* **26**, 1593 (1994).
28. R. Prangé *et al.*, *Science* **267**, 1317 (1995).

29. This work is based on observations with the National Aeronautics and Space Administration (NASA)–European Space Agency (ESA) Hubble Space Telescope, obtained at the Space Telescope Science Institute (STScI), which is operated by the AURA for NASA under contract NAS5-26555. We acknowledge R. A. West for access to near-UV images before publication, the data reduction group at the STScI for assistance in the reduction of the images, and our Comet Science Team colleagues M. McGrath and K. Noll for helpful discussions. This research was supported by grant GO-5624.18-93A from the STScI to the University of Michigan. We also acknowledge the INSU–Programme National de Planetologie, CNRS–Action Concertee Sol-Espace support, the Scientific Director of ESA for travel support for R. Prangé, and F. Paresce and D. Grodent for helpful discussions on FOC analysis.

HST Spectroscopic Observations of Jupiter After the Collision of Comet Shoemaker-Levy 9

K. S. Noll, M. A. McGrath, L. M. Trafton, S. K. Atreya, J. J. Caldwell, H. A. Weaver, R. V. Yelle, C. Barnet, S. Edgington

Ultraviolet spectra obtained with the Hubble Space Telescope identified at least 10 molecules and atoms in the perturbed stratosphere near the G impact site, most never before observed in Jupiter. The large mass of sulfur-containing material, more than 10^{14} grams in S_2 alone, indicates that many of the sulfur-containing molecules S_2, CS_2, CS, H_2S, and S^+ may be derived from a sulfur-bearing parent molecule native to Jupiter. If so, the fragment must have penetrated at least as deep as the predicted NH_4SH cloud at a pressure of approximately 1 to 2 bars. Stratospheric NH_3 was also observed, which is consistent with fragment penetration below the cloud tops. Approximately 10^7 grams of neutral and ionized metals were observed in emission, including Mg II, Mg I, Si I, Fe I, and Fe II. Oxygen-containing molecules were conspicuous by their absence; upper limits for SO_2, SO, CO, SiO, and H_2O are derived.

Ultraviolet (UV) spectroscopic observations of Jupiter were made with the Hubble Space Telescope's (HST) Faint Object Spectrograph (FOS) and Goddard High-Resolution Spectrograph (GHRS) both before and after the impacts of the fragments of periodic comet Shoemaker-Levy 9 (SL9). Four different instrument configurations were used to obtain nearly complete spectral coverage from 1250 to 3300 Å (Table 1).

Our spectroscopic program was concentrated on the area near the G impact site (*1*). All observations tracked a spot on Jupiter's surface at the position given in Table 1. Because the observations must be planned in advance, we allowed for small offsets from the best available predicted entry position of the G fragment (*2*). The actual position of the G impact was south and west of the prediction, and we adjusted the offsets accordingly. During an exposure, the position of the aperture drifts slightly in longitude and latitude because of the constant offset. The most extreme movements of the aperture occur when the target is close to a limb and amount to a drift of as much as 15° in longitude during one orbit. However, for most observations the drift is much less. Drifts in latitude are no more than 2°. Errors in pointing from uncertain guide star positions can be as large as 0.7 arc sec (1σ), or about 3° of latitude and 3° of longitude near the central meridian and as much as 10° of longitude near the limb.

One exception to our study of the G impact site occurred on 23 August when the drift of the G site carried it beyond our offset limit. We pointed instead at the predicted position of the L impact complex. The spatial distribution of dark material at the impact sites was very complex

K. S. Noll, M. A. McGrath, and H. A. Weaver are with the Space Telescope Science Institute, 3700 San Martin Drive, Baltimore, MD 21218, USA. L. M. Trafton is with the Department of Astronomy, University of Texas, Austin, TX 78712, USA. S. K. Atreya and S. G. Edgington are with the Atmospheric, Oceanic, and Space Sciences Department, University of Michigan, Ann Arbor, MI 48109, USA. J. J. Caldwell and C. Barnet are with the Institute for Space and Terrestrial Science, Space Astrophysics Laboratory, 4850 Keele Street, North York, Ontario, M3J 3K1, Canada. R. V. Yelle is with the NASA/Ames Research Center, Moffett Field, CA 94035, USA.